Saudi Journal of Biological Sciences 28 (2021) 5065–5073

Contents lists available at ScienceDirect

Saudi Journal of Biological Sciences

journal homepage: www.sciencedirect.com

Original article

Gefitinib loaded PLGA and chitosan coated PLGA nanoparticles with magnified cytotoxicity against A549 lung cancer cell lines

Abdullah S. Alshetaili *

Department of Pharmaceutics, College of Pharmacy, Prince Sattam Bin Abdulaziz University, Al-Kharj 11942, Saudi Arabia

ARTICLE INFO

Article history:
Received 8 April 2021
Revised 8 May 2021
Accepted 11 May 2021
Available online 20 May 2021

Keywords:
Gefitinib
PLGA
Chitosan
Nanoparticles
MTT assay

ABSTRACT

In the current study, gefitinib loaded PLGA nanoparticles (GFT-PLGA-NPs) and chitosan coated PLGA nanoparticles (GFT-CS-PLGA-NPs) were synthesized to investigate the role of surface charge of NPs for developing drug delivery system for non-small-cell lung cancer (NSCLC). The developed NPs were evaluated for their size, PDI, zeta potential (ZP), drug entrapment, drug loading, DSC, FTIR, XRD, *in vitro* release profile, and morphology. The anti-cancer activity of GFT loaded PLGA NPs and GFT loaded CS-PLGA-NPs were examined in human A549 lung cancer cell lines. In vitro release studies of GFT-CS-PLGA-NPs showed more sustained release in comparison to GFT-PLGA-NPs due surface charge attraction of chitosan. In addition, viability of A549 cells decreases significantly with the increasing concentration of GFT-PLGA NPs and GFT-CS-PLGA-NPs when compared to that of pure GFT and blank PLGA NPs. In addition, the microscopic analysis and counting of viable cells also validate the cytotoxicity of the developed NPs. This investigation proved that the developed NPs would be efficient carriers to deliver GFT with improved efficacy against NSCLC.

1. Introduction

Lung cancer (LC) is one of the leading causes for morbidity and mortality and considered one of the lethal forms of malignancy effecting patients' health and wellbeing (Cao et al., 2020). It remains the primary cause of cancer associated deaths globally, accountable for about 2.09 million cases in the year 2018, as per the WHO statistics report. Major lung cancer cases are interlinked to inhalation of tobacco induced products and environmental pollution besides spikes in the radiation absorbed dose due to ionized radiation leading to free radical formation and DNA mutation (Zhang et al. 2020a). LC is chiefly classified into two categories, namely non-small-cell lung cancer (NSCLC) and small cell lung cancer (SCLC). NSCLC accounts for about 85% of total lung cancer with a five-year survival rate of 4–15% due to poor prognosis.[2] The main cause of NSCLC is the overexpression of the epidermal growth factor receptor (EGFR), a member of receptor tyrosine kinase (RTK) that triggers the pathways resulting with cell-proliferation and differentiation leads to NSCLC tumour (Yang et al., 2020).

Strategies for LC treatment comprises of surgery, radiotherapy, chemotherapeutics, and radiopharmaceuticals. EGFR tyrosine kinase inhibitors (TKI) represent as standard chemotherapy for the NSCLC treatment (Quan et al., 2020). There are almost sixteen kinase inhibitors approved in the recent past for the cancer treatment. TKI chemo are drugs administered conventionally by parenteral or per oral route, and the systemic distribution of these drug without specific drug deposition in the lung may adversely affect normal tissues and organs with serious unavoidable side effects, leading to patient noncompliance and even withdrawal from the recommended dosage regimen. The EGFR tyrosine kinase inhibitors (TKI) have been used selectively for decades to treat patients of NSCLC activated by EGFR mutations.[5] Advantages of EGFR-TKIs are improved prognosis and progression free survival of NSCLC patients as compared to the cytotoxic moieties (Huang et al., 2020; Xie et al., 2020). Typically, it was observed that EGFR mutations occurs in approximately 50% of the Asian patients and 10% of the white patients with NSCLC. The drawback of EGFR-TKIs is the development of drug resistance after 10–14 months of drug induction (Yang et al., 2020). Drug resistance is self-induced by chemotherapy itself, encountered by altering the composition

* Address: Prince Sattam Bin Abdulaziz University, College of Pharmacy, P.O. Box 173 Riyadh, Al-Kharj 11942, Saudi Arabia.
E-mail address: a.alshetaili@psau.edu.sa
Peer review under responsibility of King Saud University.

Production and hosting by Elsevier

https://doi.org/10.1016/j.sjbs.2021.05.025
1319-562X/

of cancer, building more aggressiveness due to the survival of the resistant clones and modification of the genetic material, metabolism of the cancerous cells (Zhang et al., 2020a; Bouchnita et al., 2020).

NSCLC reflecting harboring of the EGFR mutation smartly treated by EGFR-TKI monotherapy. Gefitinib (GFT) is the first generation of EGFR-TKI act by blocking the signaling of EGFR via competitive ATP-binding sites. It inhibits the auto phosphorylation of EGFR, thereby blocking the transduction of downstream signals that reverse the cancer cell proliferation. Currently, GFT is used as the first line therapy for advanced NSCLC treatment (Gupta et al., 2017). GFT is a US Food and Drug Administration (FDA) approved drug intended for oral administration available in the market (Iressa®) Gefitinib tablets. GFT showed low solubility, slow absorption and poor bioavailability with pronounced side effects due to its systemic distribution. The unavoidable side effects of GFT limits its clinical implications that open new horizon for researchers to develop new nanocarriers for site specificity (Bouchnita et al., 2020). Formulation scientists explored some of the advanced drug delivery systems (DDS) with GFT such as nanoparticles (NPs), liposomes, micro-spheres, and polyurethane-foams (Zhang et al., 2020b).

Biodegradable Polymer based nanoparticles are gaining great momentum in the development of the NPs for the development of DDS of diversified drug entities (Luo et al., 2021; Allam et al., 2020). Biodegradable NPs imitates nano-size that assist the drug to permeate and cross the lipoidal biological cell membrane with consequent improvement in the solubility, permeability, absorption, and bioavailability.

Poly (lactic-co-glycolic acid) (PLGA) is a US-FDA approved biocompatible and biodegradable copolymer of polylactic and polyglycolic acid. PLGA has been extensively explored for the development of controlled DDS of small drug molecules, macromolecules such as DNA, RNA and peptides. The biodegradation of polymer depends on polymer molecular weight, ratio of lactide to glycolide, and other relevant physicochemical properties (Anzar et al., 2018). Among the various types of PLGA, PLGA 50:50 is found to biodegrade faster (Rezvantalab et al., 2018; Anwer et al., 2019; Ahmed and Badr-Eldin, 2020).

PLGA NPs imparts negative surface potential that destroy mucoadhesive property and decreases bioavailability of the drugs. The burst release and inability to accumulate drugs to target site are the major drawback of PLGA based NPs, which limits its therapeutic application. Efforts has been done on the surface modification by using chitosan (CS) to develop CS coated PLGA NPs for enhanced mucoadhesion and cellular uptake due to positive surface charge (Shim & Yoo 2020; Dyawanapelly et al., 2016; Chen et al., 2016).

The objective of the current investigation was to develop GFT-PLGA-NPs and GFT-CS-PLGA-NPs. It was expected to sustain the drug release, enhance the bioavailability, site-specificity with reduced dosage regimen. Particle characterizations include size, zeta potential, FTIR, DSC, XRD, and SEM studies to confirm the GFT loading in PLGA with surface modification by CS and the GFT release profiles and *in-vitro* anticancer study in A549 cell line.

2. Materials and method

2.1. Materials

Gefitinib (GFT) was purchased from "Mesochem Technology Co. Ltd, Beijing, China. Poly(D,L-lactide-co-glycolide) (PLGA, 50:50) and chitosan were procured from "Sigma-Aldrich, St. Louis, MO, USA". Polyvinyl alcohol (PVA, Mole wt- 85,000–124,000) was purchased from Loba Chemicals, India. "Human lung adenocarcinoma A549 (ATCC® CCL 185™) cell lines" were obtained from the American Type Culture Collection (ATCC, Manassas, VA, USA)". All chemicals/solvents used in the studies are of analytical grade.

2.2. Cell culture

The A549 cells (adenocarcinoma human alveolar basal epithelial cells) were grown in DMEM (Gibco) which were supplemented with 10% FBS (Gibco) and 1% penicillin–streptomycin (Gibco) and kept it at 37 °C, 5% CO2, and having saturated humidity. Cells were passaged in every 2 days and the logarithmic growth phase of A549 cells was taken for the MTT (3-[4,5-dimethylthiazole-2-yl]-2,5-di phenyltetrazolium bromide) test.

2.3. Preparation of GFT loaded PLGA and CS coated PLGA NPs

GFT loaded PLGA NPs were prepared by single emulsification technique. Briefly, GFT (50 mg) was dissolved in previously prepared PLGA (100 mg) polymeric solution in dichloromethane (5 mL) in order to get organic phase. On the other hand, aqueous phase containing PVA (10 mL, 0.5%, *w*/*v*) was prepared separately. The organic phase was emulsified by adding aqueous phase with syringe (0.3 mL/min) under probe sonication (probe # 423, model CL-18, Fisher scientific; United States) for 3 min at 60% W voltage efficiency. The organic solvent was evaporated on magnetic stirrer (Fisher Isotemp Hot Plate and Stirrer- Fisher scientific; USA) for 6 h. The GFT loaded PLGA NPs was collected after high speed (25, 200*g*) centrifugation and freeze dried "(Millirock Technology, Kingston, NY, USA)" after three times washing with deionized water. The GFT loaded CS-PLGA NPs were prepared using same as above procedure, except 50 mg of chitosan powder was dissolved in 1% acetic acid containing 0.5% w/v of PVA (Table 1) (Mohammed et al., 2019).

2.4. Evaluation of particle size, polydispersity index (PDI) and zeta potential (ZP)

Developed Blank PLGA-NPs, GFT loaded PLGA-NPs and GFT loaded CS-PLGA-NPs characterized for mean particle size, *PDI* and ZP. Freshly prepared colloidal dispersion was suitably diluted (200 times) with deionized water, sonicated for 10 min, and transferred into plastic disposable cuvette and measured the mean particle size and *PDI* using "Malvern zetasizer (ZEN-3600, Malvern Instruments Ltd. USA)" (Ni et al., 2017). Zeta potential of NPs were measured using "Malvern zetasizer zeta (ZEN-3600, Malvern Instruments Ltd. USA)" using glass electrode as sample holder.

2.5. Drug entrapment efficiency (%EE) and drug loading (%DL)

An indirect method was followed to measure the EE. Freshly prepared NPs dispersion was centrifuged "(HermleLabortechnik, Z216MK, Wehingen, Germany)" at 25, 200*g* for 10 min (Anwer et al., 2017). The amount of free drug was analyzed in supernatant by UV spectroscopy "(Jasco UV spectrophotometer V-630 Japan)" at λ_{max} 331 nm (Shi et al., 2014). The %EE and %DL were calculated using Equations:

$$\% \text{ EE} = \frac{(\text{Total GFT loaded} - \text{Free GFT in supernatant})}{\text{Total GFT loaded}} \times 100$$

$$\% \text{ DL} = \frac{(\text{Initially GFT added} - \text{GFT in supernatant})}{\text{Total weight of NPs}} \times 100$$

Table 1
Composition of developed NPs.

Formulae	GFT (mg)	PLGA (mg)	CS (mg)	PVA (%*w*/*v*)
Blank PLGA-NPs	–	100	–	0.5
GFT loaded PLGA-NPs	50	100	–	0.5
GFT loaded CS-PLGA-NPs	50	100	50	0.5

2.6. Differential scanning calorimetry (DSC) studies

The thermal behavior of pure GFT, GFT loaded PLGA-NPs, and GFT loaded CS-PLGA-NPs were studied by using DSC analyzer " (Shimadzu DSC-60, Shimadzu Corporation, Tokyo, Japan)". Each samples (approx. 5 mg) were crimped into aluminium pan, and subjected to heat to 250 °C at a heat rate of 20 °C/min in the presence of nitrogen gas (20 mL/min) (Sun et al., 2015).

2.7. Fourier transform infrared (FTIR) studies

FTIR spectral studies of pure GFT, GFT loaded PLGA-NPs and GFT loaded CS-PLGA-NPs were performed using "FTIR spectrometer (Jasco FTIR Spectrophotometer, Japan)". KBr technique was used to prepare a transparent pellet of each sample. FTIR spectra was recorded in the range of 4000 to 400 cm^{-1}, and peaks were interpreted using "spectral manager" software.

2.8. X-ray diffraction (XRD) studies

X-ray diffractometer "(Altima IV Regaco, Japan)" was used to record XRD pattern of the pure GFT, blank PLGA-NPs, GFT loaded PLGA-NPs and GFT loaded CS-PLGA-NPs. All samples were scanned in the angle range of 2–60° at 2θ. The scanning rate was set to 4°/min. The XRD spectra were recorded at a voltage and current of 30 kV and 25 mA, respectively (Alshdefat et al., 2020).

2.9. In-vitro release studies

In-vitro release studies of pure GFT, GFT loaded PLGA-NPs, and GFT loaded CS-PLGA-NPs were conducted at two different pH (pH 5.0 and pH 7.4). Briefly, accurately weighed amount of pure GFT (10 mg), GFT loaded PLGA-NPs and GFT loaded CS-PLGA-NPs (equivalent to 10 mg of pure GFT) were dispersed in dialysis bag "(cut off mol. weight 12,000 Dalton)" containing 5 mL of respective dissolution media with added 2% *v*/*v*, Tween 80 as surfactant. Then, dialysis bag was dipped into a beaker containing 50 mL of dissolution media, and kept on biological shaker "(LBS-030S-Lab Tech, Korea)" at 100 rpm, temperature 37 °C. At fixed time interval, 1 mL of sample was withdrawn and compensated immediately with respective media, the collected samples were analyzed for drug content after suitable dilution by UV spectroscopy at λ_{max} 331 nm (Shi et al., 2014). The release data were fitted to various kinetic models in order to know the release pattern of GFT from developed nanoparticles.

2.10. Morphology by scanning electron microscopy (SEM)

Morphological analysis of GFT loaded PLGA-NPs and GFT loaded CS-PLGA-NPs was performed by scanning electron microscopy " (Zeiss Leo 1450 SEM, Oberkochen, Germany)" operated at an accelerated voltage of 5 kV.

2.11. In vitro cytotoxicity studies- MTT assay

The cells from the logarithmic growth phase of A549 cells were seeded in the density of 2×10^4 cells per well of 96 well plate, a day before checking the cytotoxic activity of blank PLGA-NPs, GFT loaded PLGA-NPs and GFT loaded CS-PLGA-NPs. On the next day cells were washed twice with 1x PBS and replaced with fresh complete media DMEM with 10% FBS and 1% antibiotic). The different concentration of pure GFT drug (10–25 μg/mL) and formulations- blank PLGA-NPs, GFT loaded PLGA-NPs and GFT loaded CS-PLGA-NPs have added five times the concentration of pure GFT such as (50 to 125 μg/mL) and incubated it for 24 h at 37 °C. Control wells in which no drugs were added and maintained to determine the cell survival and percentage of live cells in the cell culture. After 24 h, of incubation, 10 μL of MTT (10 mg/mL) was added in each well and incubated it for 3 h at 37 °C. The yellow color of MTT is reduced to dark colored formazan only by viable cells. After the removal of medium, 200 μL of acidified isopropyl alcohol (0.04 N HCl) was added and kept on slow speed shaker at room temperature for 10 to 15 min. The color developed was quantified with an ELISA plate reader (570 nm) using Bio-Tek microplate reader (Li et al., 2019). All the experiments were performed in triplicate, and the relative cell viability (%) was expressed as a percentage relative to the untreated control cells.

2.12. Counting of cells by trypan blue and morphological changes in A549 cells

For counting the live and adhered A549 cells, cells were Trypsinsed by using 0.25% Trypsin-EDTA (Gibco), washed and resuspended in 1 mL media. 25 μL of sample was mixed with 25 μL of 0.4% trypan blue (Gibco) by gently tapping the eppendroff, and then 20 μL of the mixture was loaded into the chamber of the hemocytometer. Counting were performed under 40× objective according to standard methodology. The morphological changes in A549 cells were observed under phase contrast inverted microscope after incubating the cells for 24 h in 24 well plate and treating the cells with and without different concentration of pure GFT (10, 15, 20, and 25 μg/mL), blank PLGA-NPs, GFT loaded PLGA-NPs and GFT loaded CS-PLGA-NPs (50, 75, 100, and125 μg/mL).

3. Results

3.1. Evaluation of particle size, polydispersity index (PDI) and zeta potential (ZP)

The size, PDI, and ZP of the developed NPs are presented in Table 2. The size of the prepared NPs was found in the range of 443–527 nm. The size of GFT loaded CS-PLGA-NPs (527 nm) was measured bigger in comparison to GFT loaded PLGA-NPs (443 nm), probably due to chitosan coating on the PLGA NPs (Fig. 1). The PDI values of the prepared NPs were found in the range of 0.242–0.279, which clearly indicates the formation of monodispersed NPs. The ZP of the blank PLGA NPs, GFT loaded PLGA NPs and GFT loaded CS-PLGA-NPs were measured in negative values, −14.4 mV, −12.8 mV and +16.9 mV, respectively,

3.2. Drug entrapment efficiency (%EE) and drug loading (%DL)

The EE and DL of GFT loaded PLGA-NPs were measured as 85.65% and 2.15%, respectively. However, EE and DL for GFT loaded

Table 2
Particle characterization and encapsulation efficiencies of the developed NPs.

Formulae	Particle Size (nm) ± SD	PDI	ZP (mV)	%EE ± SD	%DL ± SD
Blank PLGA-NPs	443 ± 5.4	0.261 ± 0.06	−14.4 ± 2.1	–	
GFT loaded PLGA-NPs	489 ± 4.1	0.242 ± 0.02	−12.8 ± 1.8	85.65 ± 3.7	2.15 ± 0.24
GFT loaded CS-PLGA-NPs	527 ± 6.3	0.279 ± 0.04	+16.9 ± 0.7	82.46 ± 5.2	2.34 ± 0.16

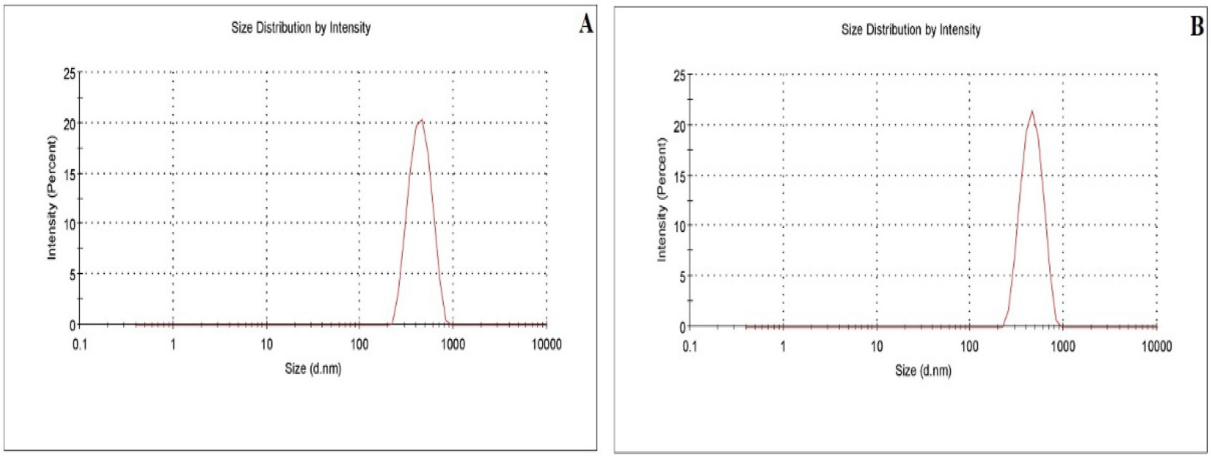

Fig. 1. Particle size measured by diffraction light scattering (DLS) technique. (**A**)—GFT loaded PLGA-NPs; (**B**)—GFT loaded CS-PLGA-NPs.

CS-PLGA-NPs were measured as 82.46% and 2.34%, respectively (Table 2).

3.3. Differential scanning calorimetry (DSC) studies

A comparative DSC spectrum of pure GFT, GFT loaded PLGA-NPs, and GFT loaded CS-PLGA-NPs are shown in Fig. 2. The DSC spectra of pure GFT showed a sharp endothermic peak at 199 °C as reported in literature (Gidwani et al., 2018). A diminished endothermic peak of GFT was observed in GFT loaded PLGA-NPs. A broad endothermic peak of PLGA could be seen near 85 °C in GFT loaded PLGA-NPs, that is completely disappeared in GFT loaded CS-PLGA-NPs, probably due to coating of chitosan over PLGA NPs. However, no peak of GFT was observed in GFT loaded CS-PLGA-NPs, which indicated the complete encapsulation of GFT in polymer.

3.4. Fourier transform infrared (FTIR) studies

The FTIR spectra of pure GFT, GFT loaded PLGA-NPs and GFT loaded CS-PLGA-NPs are shown in Fig. 3. In the spectra pure GFT, typical peaks at 2866 cm^{-1} is attributed to the O—H stretching, 1709 cm^{-1} for C═O, 1625 cm^{-1} for C═N stretching 1113 cm^{-1} for C—O stretching and 1010 for C-F stretching (Liu et al., 2017). Compared to the pure GFT, absorption peaks at fingerprint region (1600–400 cm^{-1}) were disappeared or weakened in both GFT

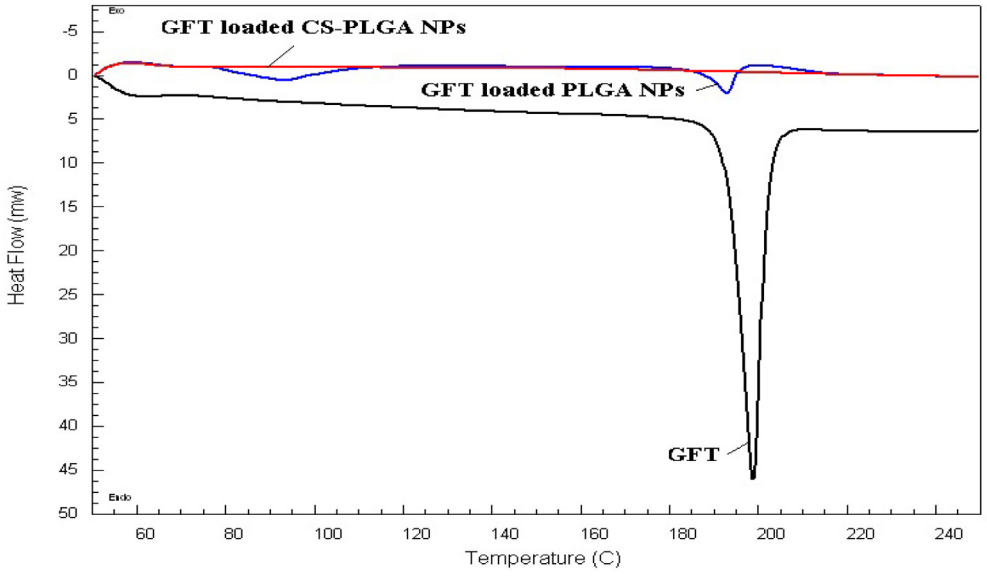

Fig. 2. Comparative DSC thermograms of pure GFT and developed nanoparticles.

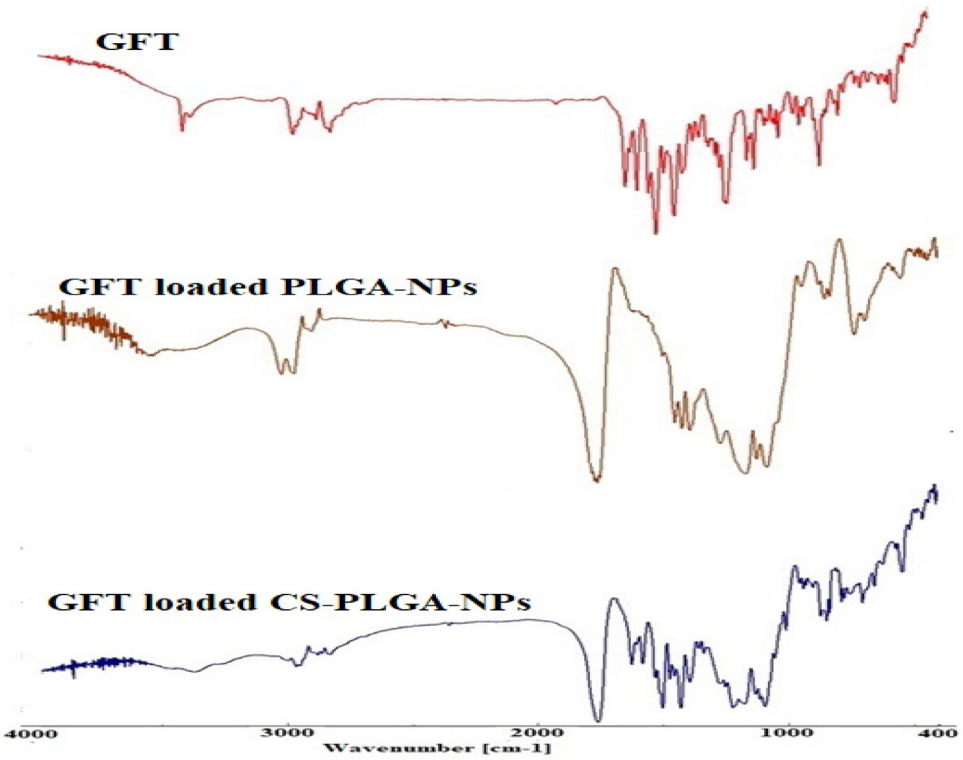

Fig. 3. Comparative FTIR spectra of pure GFT and developed nanoparticles.

loaded PLGA-NPs and GFT loaded CS-PLGA-NPs, indicating a successful entrapment of the drug inside polymeric matrix.

3.5. X-ray diffraction (XRD) studies

X-ray diffractometer pattern of pure GFT, blank PLGA-NPs, GFT loaded PLGA-NPs and GFT loaded CS-PLGA-NPs are shown in Fig. 4. Pure GFT showed characteristic intense peaks at 19.3°, 20.6°, 22.5°, 24°, 38.1° and 44.3° as reported in literature (Chen et al., 2017). The sharp peaks of GFT disappeared completely in GFT loaded PLGA-NPs and GFT loaded CS-PLGA-NPs, indicating that GFT was dispersed molecularly with the polymer in NPs.

The dissolution behavior of free GET, GFT loaded PLGA-NPs and GFT loaded CS-PLGA-NPs examined in two buffer at pH 5.0 and 7.4 (Fig. 5). Free GFT drug was released quickly in both dissolution media. In contrast, an initial burst drug release on 2 h was observed as 68.2% and 56.4% at pH 5.0, 50%, 42.6% at pH 7.4, from GFT loaded PLGA-NPs and GFT loaded CS-PLGA-NPs, respectively.

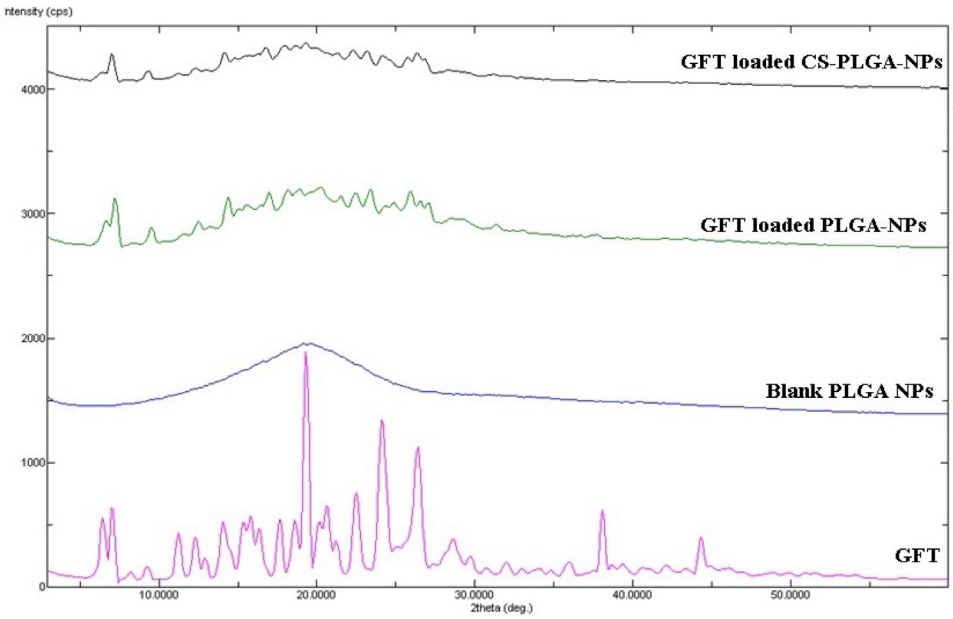

Fig. 4. Comparative XRD spectra of pure GFT and developed nanoparticles.

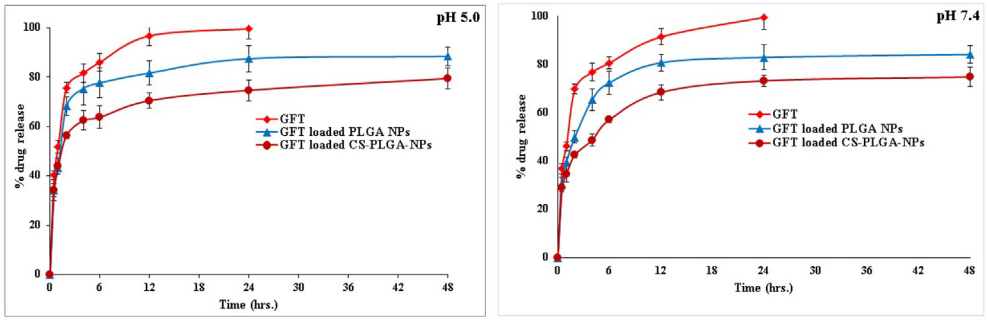

Fig. 5. Comparative release profile of pure GFT and developed nanoparticles.

The initial burst release of drug from NPs could be due to presence of free or adsorbed surface drug. The burst release may reduce the efficacy and causes adverse effects. The strong burst release was reduced and sustained in both GFT loaded PLGA-NPs and GFT loaded CS-PLGA-NPs to enhance the efficacy of drug. However, due to charge attraction between drug and chitosan in GFT loaded CS-PLGA-NPs exhibited more sustained release of drug in comparison to GFT loaded PLGA-NPs (Fig. 5) (Chen et al., 2017). The release data was fitted to various kinetic models in order to know release mechanism of GFT from GFT loaded PLGA-NPs and GFT loaded CS-PLGA-NPs. Based on best fitted correlation coefficients (R^2), the developed polymeric nanoparticles followed the Krosmeyer–Peppas model with R^2 values 0.9791 (pH 5.0), 0.9805 (pH 7.4) and 0.9780 (pH 5.0), 0.9804 (pH 7.4) for GFT loaded PLGA-NPs and GFT loaded CS-PLGA-NPs, respectively. The kinetic data indicated simultaneous release mechanism of GFT by diffusion of water into polymer, swelling of the polymeric matrix, and dissolution (Supramaniam et al., 2018).

3.6. Morphology by scanning electron microscopy (SEM)

Surface morphology of freeze dried GFT loaded PLGA-NPs was observed smooth and spherical in shape with aggregation. However, GFT loaded CS-PLGA-NPs were observed as rough spherical aggregated particles, probably due to coating of chitosan on PLGA nanoparticles. The size of GFT loaded PLGA-NPs and GFT loaded CS-PLGA-NPs particles was found to be close to DLS measured particles (Fig. 6).

3.7. In vitro cytotoxicity studies- MTT assay

The cytotoxicity activity of pure GFT, blank PLGA NPs, GFT loaded PLGA NPs, and GFT loaded CS-PLGA-NPs were performed on A549 lung cancer cells using MTT assay, as discussed in detail in material and methods section. The histogram plot of the percentage of cell viability versus the different concentrations of drugs is presented in Fig. 7. To determine the effectiveness of formulated nanoparticles, GFT loaded PLGA NPs, and GFT loaded CS-PLGA-NPs as compared to the pure GFT, blank PLGA NPs, we performed a cell viability assay on A549 cells with different concentrations of blank PLGA NPs, GFT loaded PLGA NPs, and GFT loaded CS-PLGA-NPs were taken five times that of pure GFT concentration. Both GFT loaded PLGA NPs and GFT loaded CS-PLGA-NPs illustrated a significant decrease in cell viability at concentration from 50 to 125 μg/ml.

* $p < 0.005$ highly significant. Compared between control vs. A, B, C and D at all concentration. # $p < 0.005$ highly significant. Compared between A treated with 10 μg/mL vs. B, C and D nanoparticles having 50 μg/mL concentration. Similarly, † $p < 0.005$ highly significant. Compared between the A treated with 15 μg/mL vs. B, C and D nanoparticles having 75 μg/mL concentration. ¥ $p < 0.005$ highly significant. Compared between A treated with 20 μg/mL vs. B, C and D nanoparticles having 100 μg/mL concentration. £ $p < 0.005$ Highly significant. Compared between A treated with 25 μg/mL vs. B, C and D nanoparticles having 125 μg/mL concentration.

3.8. Counting of cells by trypan blue and morphological changes in A549 cells

The cytotoxicity activity of pure GFT, blank PLGA-NPs, GFT loaded PLGA-NPs and GFT loaded CS-PLGA-NPs were performed with A549 cells using MTT assay, as discussed in detail in material and methods. The histogram plot of the percentage of cell survival versus the different concentrations of drugs is presented in Fig. 7. To determine the effectiveness of formulated nanoparticles GFT loaded PLGA-NPs and GFT loaded CS-PLGA-NPs as compared to the pure GFT and blank PLGA-NPs, cell viability assay was per-

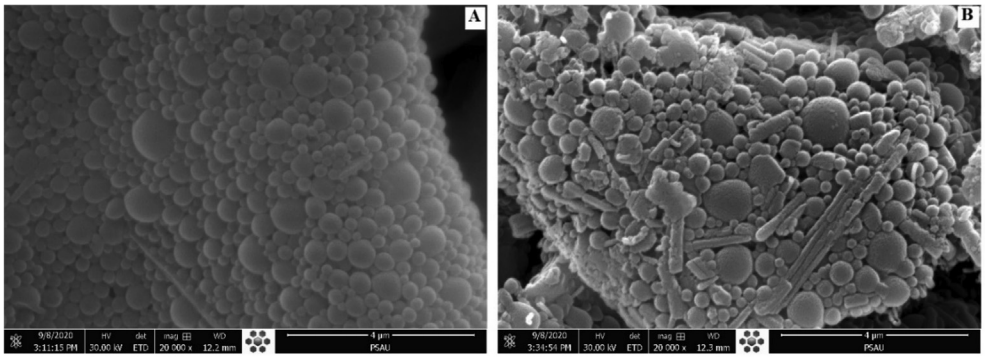

Fig. 6. SEM images; (**A**)—GFT loaded PLGA-NPs; (**B**)—GFT loaded CS-PLGA-NPs.

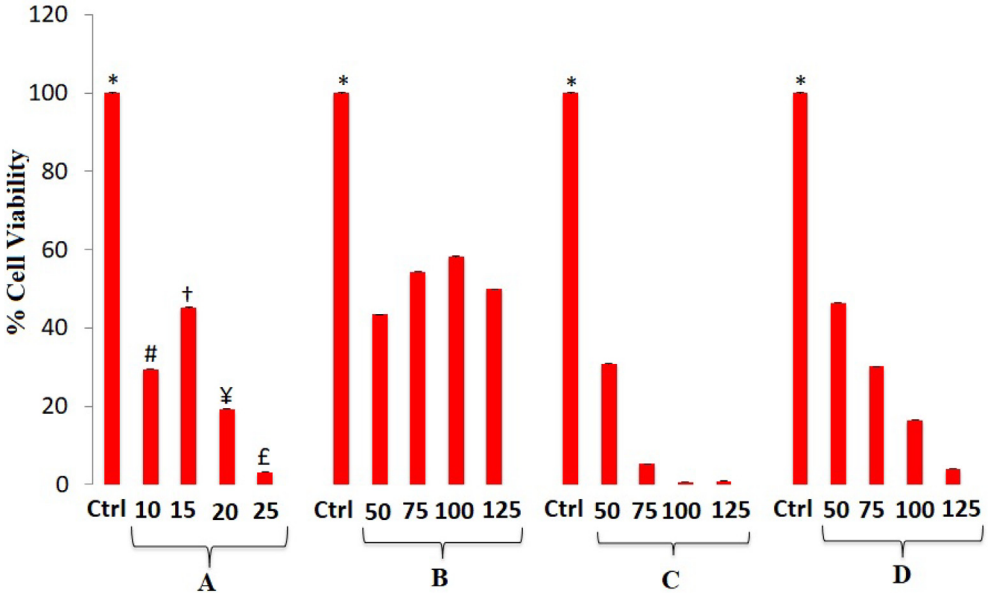

Fig. 7. Viability of A549 cells after 24 h exposure to varying concentration (10–25 ng/mL) of pure GFT and their five times concentration (50–125 ng/mL) of blank PLGA NPs, GFT loaded PLGA NPs, and GFT loaded CS-PLGA-NPs determined by MTT assay. The data are expressed as the mean of two independent experiments and error bars represents the standard deviation. (**A**)—pure GFT; (**B**)—blank PLGA NPs; (**C**)—GFT-CS-PLGA-NPs; (**D**)—GFT-PLGA-NPs.

formed on A549 cells with different concentrations of pure GFT, blank PLGA-NPs, GFT loaded PLGA-NPs and GFT loaded CS-PLGA-NPs. The viability of A549 cells decreases significantly with the increasing concentration of pure GFT loaded PLGA-NPs and GFT loaded CS-PLGA-NPs when compared to that of GFT, blank PLGA-NPs. Based on the above result of the MTT assay, the percentage of A549 cell viability decreases with the increasing concentration of GFT loaded CS-PLGA-NPs. The microscopic analysis as shown in Fig. 8 and counting of viable cells as shown in Table 3 validates the cytotoxicity of developed NPs The morphological changes of A549 lung cancer, when treated with PLGA-NPs, GFT loaded PLGA-NPs and GFT loaded CS-PLGA-NPs with increasing concentration (50–125 μg/ml), apoptosis and generation of debris were observed with a marked cell number reduction (Table 3), the cells

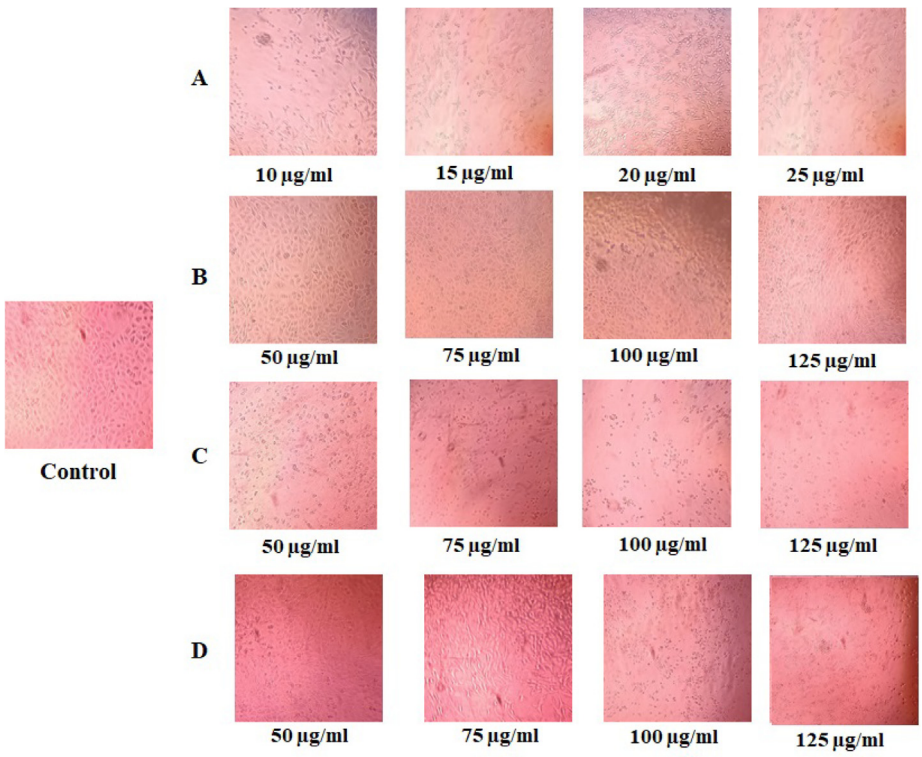

Fig. 8. Phase contrast images of morphological changes observed in A549 cells after exposure of different concentrations. (**A**)—pure GFT; (**B**)—blank PLGA NPs; (**C**)—GFT-CS-PLGA-NPs; (**D**)—GFT-PLGA-NPs.

Table 3
Live cells counting by Trypan blue staining after 24 h treatments.

Control (Cell Count/mL)	Conc. (μg/mL)	Pure GFT (Cell Count/mL)	Conc. (μg/mL)	Blank PLGA-NPs (Cell Count/mL)	GFT Loaded PLGA-NPs (Cell Count/mL)	GFT Loaded CS-PLGA-NPs (Cell Count/mL)
5×10^4	10	2.1×10^4	50	3.0×10^4	3.0×10^4	2.3×10^4
	15	2.7×10^4	75	3.2×10^4	2.4×10^4	1.1×10^4
	20	1.4×10^4	100	3.0×10^4	1.5×10^4	1.0×10^4
	25	1.2×10^4	125	2.8×10^4	1.0×10^4	1.0×10^4

experienced maximum changes with increasing concentration of GFT loaded CS-PLGA-NPs in the morphology, apoptosis and generation of debris as shown in Fig. 8 as compared to pure GFT, blank PLGA-NPs, and GFT loaded PLGA-NPs.

4. Discussion

The purpose of this study was to develop GFT-PLGA-NPs and GFT-CS-PLGA-NPs and magnify the activity of GFT by enhancing bioavailability and sustainability in the treatment of non-small cell lung cancer. The large dose, side effects and non-targeting limits the therapy in lung cancer. The PLGA and chitosan coated PLGA NPs could be a novel alternatives to overcome these problems by enabling delivery of GFT to the target site (Arafa et al., 2020; Nafee et al., 2007).

GFT loaded PLGA NPs and GFT-CS-PLGA-NPs were prepared by single emulsification technique (Anwer et al., 2019). The developed NPs were evaluated for their particle characteristics, and particle size, PDI and ZP were measured as 489 nm, 0.242 and −12.8 mV for GFT loaded PLGA NPs and 527 nm, 0.279 and +16.9 mV for GFT-CS-PLGA-NPs, respectively (Table 2). This size of the particles greatly influences the tumour targeting of anti-cancer drugs by various means including circulation, biodistribution, accumulation, and penetration mechanism (Dadwal et al., 2018). The ZP of the blank PLGA NPs and GFT loaded PLGA NPs were measured in negative values, −14.4 mV and −12.8 mV, respectively, the negative values of ZP was measured due to carboxylic group present on the surface of PLGA polymer (Kocbek, et al., 2007). However, ZP of GFT loaded CS-PLGA NPs were measured in positive value (+16.9 mV), probably due to the presence of an amino group of chitosan on the surface of NPs, which indicated a successful surface coating of chitosan on PLGA NPs. Due to surface coating of chitosan over PLGA nanoparticles, zeta potential of the PLGA nanoparticle surface changed from a negative charge to positive value, making the drug carriers have a greater affinity to lung cancer cells (Shukla et al, 2014). The high drug encapsulations were observed both in GFT loaded PLGA-NPs and GFT loaded CS-PLGA-NPs, probably due to a reduction of drug leakage from NPs (Table 2). DSC, FTIR and XRD analysis of GFT loaded PLGA NPs and GFT-CS-PLGA-NPs suggested the absence of free crystalline GFT and complete encapsulation within polymer. The *in vitro* drug release studies showed burst release initially from NPs could be due to presence of free or adsorbed surface drug (Anwer et al., 2019). The burst release may reduce the efficacy and causes adverse effects. The strong burst release was reduced and sustained in both GFT loaded PLGA-NPs and GFT loaded CS-PLGA-NPs to enhance the efficacy of drug. However, due to charge attraction between drug and chitosan in GFT loaded CS-PLGA-NPs exhibited more sustained release of drug in comparison to GFT loaded PLGA-NPs (Fig. 5) (Chen et al., 2017). Surface morphology of the NPs were studied by SEM, and found spherical in shape.

In cell viability study, GFT loaded PLGA NPs and GFT loaded CS-PLGA-NPs showed a decrease in cell viability from 46 to 4% and 31 to 0.9%, respectively, against A549 cell lines. Based on the above results, the maximum decrease in percentage cell viability was observed with GFT loaded CS-PLGA-NPs in comparison to other formulae.

In addition, the microscopic analysis and counting of viable cells also supports the cytotoxicity data of cytotoxicity studies against A549 cell lines. A marked reduction in cell number was observed.

5. Conclusions

In conclusion, GFT loaded PLGA-NPs and GFT loaded CS-PLGA-NPs were prepared using a single emulsion and evaporation technique, and NPs formation was confirmed by particle characterization, *in vitro* release studies, and MTT assay against lung cancer cell lines. The developed NPs benefits from their nano-size and positive surface charge of chitosan that promise a magnified efficacy against lung cancer. The GFT loaded CS-PLGA NPs offers a unique formulation approach to sustained the drug release with better efficacy against A549 lung cancer cell line.

Declaration of Competing Interest

The authors declare that they have no known competing financial interests or personal relationships that could have appeared to influence the work reported in this paper.

Acknowledgments

"This publication was supported by the Deanship of Scientific Research at Prince Sattam Bin Abdulaziz University, Al-Kharj Saudi Arabia. The author wish to thank laboratory technician for their technical assistance with the spectral and SEM studies and Md. Khalid Anwer for his helpful suggestions and discussion.

References

Ahmed, O., Badr-Eldin, S.M., 2020. Biodegradable self-assembled nanoparticles of PEG-PLGA amphiphilic diblock copolymer as a promising stealth system for augmented vinpocetine brain delivery. Int. J. Pharm. 588,. https://doi.org/10.1016/j.ijpharm.2020.119778 119778.

Allam, H.A., Aly, E.E., Farouk, A., El Kerdawy, A.M., Rashwan, E., Abbass, S., 2020. Design and Synthesis of some new 2,4,6-trisubstituted quinazoline EGFR inhibitors as targeted anticancer agents. Bioorg. Chem. 98,. https://doi.org/10.1016/j.bioorg.2020.103726 103726.

Alshdefat, R., Anwer, M.K., Fayed, M.H., Alsulays, B.B., Tawfeek, H.M., Abdel-Rahman, R.F., Soliman, G.A., 2020. Preparation and evaluation of spray dried rosuvastatin calcium-PVP microparticles for the improvement of serum lipid profile. J. Drug. Deliv. Sci. Technol. 55,. https://doi.org/10.1016/j.jddst.2019.101342 101342.

Anwer, M.K., Al-Shdefat, R., Ezzeldin, E., Alshahrani, S.M., Alshetaili, A.S., Iqbal, M., 2017. Preparation, evaluation and bioavailability studies of eudragit coated PLGA nanoparticles for sustained release of eluxadoline for the treatment of irritable bowel syndrome. Front. Pharmacol. 8, 844. https://doi.org/10.3389/fphar.2017.00844.

Anwer, M.K., Mohammad, M., Ezzeldin, E., Fatima, F., Alalaiwe, A., Iqbal, M., 2019. Preparation of sustained release apremilast-loaded PLGA nanoparticles: in vitro characterization and *in vivo* pharmacokinetic study in rats. Int. J. Nanomed. 14, 1587–1595. https://doi.org/10.2147/IJN.S195048.

Anzar, N., Mirza, M.A., Anwer, M.K., Khuroo, T., Alshetaili, A.S., Alshahrani, S.M., Meena, J., Hasan, N., Talegaonkar, S., Panda, A.K., Iqbal, Zeenat, 2018. Preparation, evaluation and pharmacokinetic studies of spray dried PLGA polymeric submicron particles of simvastatin for the effective treatment of breast cancer. J. Mol. Liq. 249, 609–616. https://doi.org/10.1016/j.molliq.2017.11.081.

Arafa, M.G., Girgis, G., El-Dahan, M.S., 2020. Chitosan-coated PLGA nanoparticles for enhanced ocular anti-inflammatory efficacy of atorvastatin calcium. Int. J. Nanomed. 15, 1335–1347. https://doi.org/10.2147/IJN.S237314.

Bouchnita, A., Volpert, V., Koury, M.J., Hellander, A., 2020. A multiscale model to design therapeutic strategies that overcome drug resistance to tyrosine kinase inhibitors in multiple myeloma. Math. Biosci. 319,. https://doi.org/10.1016/j.mbs.2019.108293 108293.

Cao, L., Hong, W., Cai, P., et al., 2020. Cryptotanshinone strengthens the effect of gefitinib against non-small cell lung cancer through inhibiting transketolase. Eur. J. Pharmacol. 173647. https://doi.org/10.1016/j.ejphar.2020.173647.

Chen, H., Xie, L.Q., Qin, J., Jia, Y., Cai, X., Nan, W., Yang, W., Lv, F., Zhang, Q.Q., 2016. Surface modification of PLGA nanoparticles with biotinylated chitosan for the sustained in vitro release and the enhanced cytotoxicity of epirubicin. Colloids Surf. B, Biointerfaces. 138, 1–9. https://doi.org/10.1016/j.colsurfb.2015.11.033.

Chen, W., Clauser, J., Thiebes, A.L., McGrath, D.J., Kelly, N., van Steenbergen, M.J., Jockenhoevel, S., Steinseifer, U., McHugh, P.E., Hennink, W.E., Kok, R.J., 2017. Gefitinib/gefitinib microspheres loaded polyurethane constructs as drug-eluting stent coating. Eur. J. Pharm. Sci. 103, 94–103. https://doi.org/10.1016/j.ejps.2017.02.002.

Dadwal, A., Baldi, A., Kumar Narang, R., 2018. Nanoparticles as carriers for drug delivery in cancer. Artif. Cells Nanomed. Biotechnol. 46, 295–305. https://doi.org/10.1080/21691401.2018.1457039.

Dyawanapelly, S., Koli, U., Dharamdasani, V., Jain, R., Dandekar, P., 2016. Improved mucoadhesion and cell uptake of chitosan and chitosan oligosaccharide surface-modified polymer nanoparticles for mucosal delivery of proteins. Drug. Deliv. Trans. Res. 6, 365–379. https://doi.org/10.1007/s13346-016-0295-x.

Gidwani, B., Vyas, A., Kaur, C.D., 2018. Investigation of inclusion behaviour of gefitinib with epichlorohydrin-β-cyclodextrin polymer: preparation of binary complex, stoichiometric determination and characterization. J. Pharm. Biomed. Anal. 160, 31–37. https://doi.org/10.1016/j.jpba.2018.07.025.

Gupta, M., Marwaha, R.K., Dureja, H., 2017. Development and characterization of gefitinib loaded polymeric nanoparticles by ionic gelation method. Pharm. Nanotechnol. 5, 301–309. https://doi.org/10.2174/2211738505666171004124109.

Huang, Y., Dai, Y., Wen, C., Zhao, D., Wu, L., Zhou, H., 2020. circSETD3 contributes to acquired resistance to gefitinib in non-small-cell lung cancer by targeting the miR-520h/ABCG2 pathway. Mol. Ther - Nucleic Acids. 21, 885–899. https://doi.org/10.1016/j.omtn.2020.07.027.

Kocbek, P., Obermajer, N., Cegnar, M., Kos, J., Kristl, J., 2007. Targeting cancer cells using PLGA nanoparticles surface modified with monoclonal antibody. J. Contrl. Rel. 120, 18–26. https://doi.org/10.1016/j.jconrel.2007.03.012.

Li, X., Wang, J., Li, S., Liu, Z., Zheng, Z., Zhang, Y., 2019. Development and evaluation of multifunctional poly(lactic-co-glycolic acid) nanoparticles embedded in carboxymethyl β-glucan porous microcapsules as a novel drug delivery system for gefitinib. Pharmaceutics. 11, 469. https://doi.org/10.3390/pharmaceutics11090469.

Liu, G., Lin, Q., Huang, Y., Guan, G., Jiang, Y., 2017. Tailoring the particle microstructures of gefitinib by supercritical CO2 anti-solvent process. J. CO2 Util. 20, 43–51. https://doi.org/10.1016/j.jcou.2017.04.015.

Luo, M., Hua, S., Shang, Q., 2021. Application of nanotechnology in drug delivery systems for respiratory diseases (Review). Mol. Med. Rep. 23, 325. https://doi.org/10.3892/mmr.2021.11964.

Mohammed, M., Alnafisah, M.S., Anwer, M.K., Fatima, F., Almutairy, B.K., Alshahrani, S.M., Alshetaili, A.S., Alalaiwe, A., Fayed, M.H., Alanazi, A.Z., Alzahrani, M., Hailat, M.M., Alshdefat, R., 2019. Chitosan surface modified PLGA nanoparticles loaded with brigatinib for the treatment of non-small cell lung cancer. J. Polym. Engn. 39, 909–916. https://doi.org/10.1515/polyeng-2019-0265.

Nafee, N., Taetz, S., Schneider, M., Schaefer, U.F., Lehr, C.M., 2007. Chitosan-coated PLGA nanoparticles for DNA/RNA delivery: effect of the formulation parameters on complexation and transfection of antisense oligonucleotides. Nanomed. 3 (3), 173–183. https://doi.org/10.1016/j.nano.2007.03.006.

Ni, X.L., Chen, L.X., Zhang, H., Yang, B., Xu, S., Wu, M., Liu, J., Yang, L.L., Chen, Y., Fu, S. Z., Wu, J.B., 2017. *In vitro* and *in vivo* antitumor effect of gefitinib nanoparticles on human lung cancer. Drug Deliv. 24, 1501–1512. https://doi.org/10.1080/10717544.2017.1384862.

Quan, C., Chen, Y., Wang, X., et al., 2020. Loss of histone lysine methyltransferase EZH2 confers resistance to tyrosine kinase inhibitors in non-small cell lung cancer. Cancer Lett. 495, 41–52. https://doi.org/10.1016/j.canlet.2020.09.003.

Rezvantalab, S., Drude, N.I., Moraveji, M.K., Güvener, N., Koons, E.K., Shi, Y., Lammers, T., Kiessling, F., 2018. PLGA-based nanoparticles in cancer treatment. Front. Pharmacol. 9, 1260. https://doi.org/10.3389/fphar.2018.01260.

Shi, Y., Su, C., Cui, W., et al., 2014. Gefitinib loaded folate decorated bovine serum albumin conjugated carboxymethyl-beta-cyclodextrin nanoparticles enhance drug delivery and attenuate autophagy in folate receptor-positive cancer cells. J. Nanobiotechnol. 12, 43. https://doi.org/10.1186/s12951-014-0043-7.

Shim, S., Yoo, H.S., 2020. The application of mucoadhesive chitosan nanoparticles in nasal drug delivery. Mar. Drugs 18 (12), 605. https://doi.org/10.3390/md18120605.

Shukla, S., Jadaun, A., Arora, V., Sinha, R.K., Biyani, N., Jain, V.K., 2014. In vitro toxicity assessment of chitosan oligosaccharide coated iron oxide nanoparticles. Toxicol. Rep. 2, 27–39. https://doi.org/10.1016/j.toxrep.2014.11.002.

Sun, S.B., Liu, P., Shao, F.M., Miao, Q.L., 2015. Formulation and evaluation of PLGA nanoparticles loaded capecitabine for prostate cancer. Int. J. Clin. Expt. Med. 8 (10), 19670–19681.

Supramaniam, J., Adnan, R., Mohd Kaus, N.H., Bushra, R., 2018. Magnetic nanocellulose alginate hydrogel beads as potential drug delivery system. Int. J. Biol. Macromol. 118, 640–648. https://doi.org/10.1016/j.ijbiomac.2018.06.043.

Xie, Y.J., Gao, W.N., Wu, Q.B., et al., 2020. Chelidonine selectively inhibits the growth of gefitinib-resistant non-small cell lung cancer cells through the EGFR-AMPK pathway. Pharmacol. Res. 159, 104934. https://doi.org/10.1016/j.phrs.2020.104934.

Yang, Y.M., Jang, Y., Lee, S.H., Kang, B., Lim, S.M., 2020a. AXL/MET dual inhibitor, CB469, has activity in non-small cell lung cancer with acquired resistance to EGFR TKI with AXL or MET activation. Lung Cancer. 146, 70–77. https://doi.org/10.1016/j.lungcan.2020.05.031.

Yang, J.C., Cheng, Y., Murakami, H., Yang, P.C., He, J., Nakagawa, K., Kang, J.H., Kim, J. H., Hozak, R.R., nguyen, T.S., Zhang, W.L., Enatsu, S., Puri, T., Orlando, M., 2020b. A randomized phase 2 study of gefitinib with or without pemetrexed as first-line treatment in nonsquamous NSCLC with EGFR mutation: final overall survival and biomarker analysis. J. Thor. Oncol. 15, 91–100. https://doi.org/10.1016/j.jtho.2019.09.008.

Zhang, T., Bao, J., Zhang, M., et al., 2020a. Chemo-photodynamic therapy by pulmonary delivery of gefitinib nanoparticles and 5-aminolevulinic acid for treatment of primary lung cancer of rats. Photodiagn. Photodyn. Ther. 101807. https://doi.org/10.1016/j.pdpdt.2020.101807.

Zhang, T., Wang, R., Li, M., Bao, J., Chen, Y., Ge, Y., Jin, Y., 2020b. Comparative study of intratracheal and oral gefitinib for the treatment of primary lung cancer. Eur. J. Pharm. Sci. 149,. https://doi.org/10.1016/j.ejps.2020.105352 105352.